Mini Review

iMedPub Journals
www.imedpub.com

Insights in Analytical Electrochemistry
ISSN 2470-9867

2020
Vol.6 No.1:2

DOI: 10.36648/2470-9867.6.1.2

Electrochemical Characterization of Al86Ce10TM4 (TM=Fe, Co, Ni and Cu) Amorphous Alloys

Jianqi Zhang[1*], Yichao Fu[2], Tian Zhang[1], August Chang[3], Wenwen Li[1], Pengzhong Shi[1], Na Na[1], Chenyuan Chang[1], Jiyu Jia[1], Dianchen Feng[1], Xuemei Wang[1], Yinfeng Zhao[1], Tao Li[1], Yongchang Huang[4] and Shengli An[1]

[1]Inner Mongolia University of Science and Technology, Baotou 014010, P R China

[2]Hohai University, Nanjing 210098, P R China

[3]University of Wisconsin-Madison, Madison, Wisconsin 53706, USA

[4]Shanghai Jiaotong University, Shanghai 200240, P R China

[*]**Corresponding author:** Jianqi Zhang, Inner Mongolia University of Science and Technology, Baotou 014010, P R China, E-mail: jzhang82@imust.cn

Received date: January 29, 2020; **Accepted date:** February 11, 2020; **Published date:** February 18, 2020

Citation: Zhang J, Fu Y, Zhang T, Chang A, Li W, et al. (2020) Electrochemical Characterization of Al86Ce10TM4 (TM=Fe, Co, Ni and Cu) Amorphous Alloys. Insights Anal Electrochem Vol 6 No.1:2.

Abstract

Electrochemical behavior of Al86Ce10TM4 (TM=Fe, Co, Ni and Cu) amorphous alloys was studied. The amorphous alloys exhibit corrosion resistance and mechanical hardness substantially higher than the traditional Al alloys on merit of electrochemical homogeneity, self-passivating and lattice strengthening of the amorphous matrix. Annealing crystallization of the amorphous alloys can furthermore promote these properties significantly due to the added effect of metallic nano-crystals tessellated in the amorphous matrix in mechanisms of anti-corrosion enhancement and precipitate hardening. The oxide films grown on the amorphous alloys at 630°C in static air provide superior corrosion resistance due to the resilient blockage of the oxide layers to the environment. The results manifest amorphous Al86Ce10TM4 (TM=Fe, Co, Ni and Cu) alloys present distinguished electrochemical and mechanical properties and thus have potential aerospace and defence applications in terms of their mechanical strength (800~1200 MPa), high temperature endurance (300~420°C and anti-oxidation (630°C) and corrosion resistance (10-6~10-8 A/cm2).

Keywords: Amorphous Alloys; Al-Ce-TM; Devitrification; Oxidation; Corrosion

Introduction

Over the past three decades since Poon [1] and Inoue [2] reported Al-based amorphous alloys with high tensile strength and good ductility in 1988, the Al-based amorphous alloys have allured great interest in terms of their peculiar mechanical properties in comparison to traditional Al alloys [3-5]. Investigations on glass forming ability, thermal stability, devitrification, microstructure and property [6-12] have become the centered topics thus far.

Besides superior mechanical performance, electrochemical behavior of the Al-based amorphous alloys has also become the focused study as corrosion resistance is always taken regard as one of the major criteria for practical applications under variant environments such as land, sea or space. Quite a few reports have been published in the past years [13-16]. In this communication, we aim to summarize our research regarding the electrochemical characterization of the Al86Ce10TM4 (TM=Fe, Co, Ni and Cu) alloys in amorphous state, through devitrification process and to the oxide layers formed by high temperature oxidation.

Experimental

Amorphous Al86Ce10TM4 (TM=Fe, Co, Ni and Cu) tapes were fabricated by melt-spin method. All the as-spun tapes were 40 μm thick and 4 mm wide. The morphology, composition and structure were examined by transmission electron microscope, scanning electron microscope and energy dispersive spectroscopy, and X-ray diffraction. Devitrification of the as-spun tapes was studied by differential scanning calorimeter and carried out at designated temperatures under flowing high-purity argon [17,18]. Oxidation was conducted at 630°C in static air. The mechanical and electrochemical behaviors of the alloys and oxide films were measured using an indentation tester and a Solartron electrochemical interface. All measurements were repeated five times, and the average values were utilized as the final results with the uncertainty estimates determined by the least square method.

Results and Discussion

Figure 1 illustrates the potentiodynamic polarizations of the as-spun Al86Ce10TM4 (TM= Fe, Co, Ni and Cu) alloys measured in 3.56 wt.%NaCl aqueous solution. The measured parametric data are summarized in **Table 1**. The as-spun alloys have been identified to be a full amorphous matrix embedded with short range ordered (SRO) quasi-crystalline clusters [17,18]. Compared to pure Al or the traditional Al alloys such as AA 2024, AA 6061 and AA 7075 [4], the as-spun amorphous alloys not only exhibit enhanced mechanical hardness (Hv) but also improved corrosion resistance. As compared to the parametric data of pure Al, the corrosion (Ecorr) and pitting (Epit) potentials of the amorphous Al86Ce10TM4 (TM= Fe, Co, Ni and Cu) alloys are more noble while the passivation current density (Ipass) dwindles and localized corrosion susceptibility (ΔErep) drops except Al86Ce10Cu4. The higher mechanical hardness of the amorphous alloys than the traditional crystalline counterparts relies essentially on the amorphous matrix of the former, whose disordered and tortured atomic lattices generate lots of internal stress and strain, making the amorphous matrix tougher than the crystalline ones. In addition, the amorphous matrix are further strengthened by solute (Ce and TM) and precipitation (SRO clusters) hardening, conferring the amorphous matrix superior hardness to the crystalline alloys. The excellent electrochemical behavior should be also ascribed to the amorphous matrix that is not only natively self-passivating but also electrochemically homogeneous, offering peculiar resistance to generalized and localized corrosions.

To inspect how devitrification of the amorphous matrix in association with the mechanical and electrochemical performance evolves, the as-spun alloys were annealed at designated temperatures (the first crystallization onset and end temperatures and the second crystallization onset temperature, for which polarization curves are marked in black, red and blue, respectively) for 15 minutes in Ar atmosphere [17,18]. **Figure 2** depicts the electrochemical polarizations of the post-annealed alloys with the measured data provided in **Table 1.**

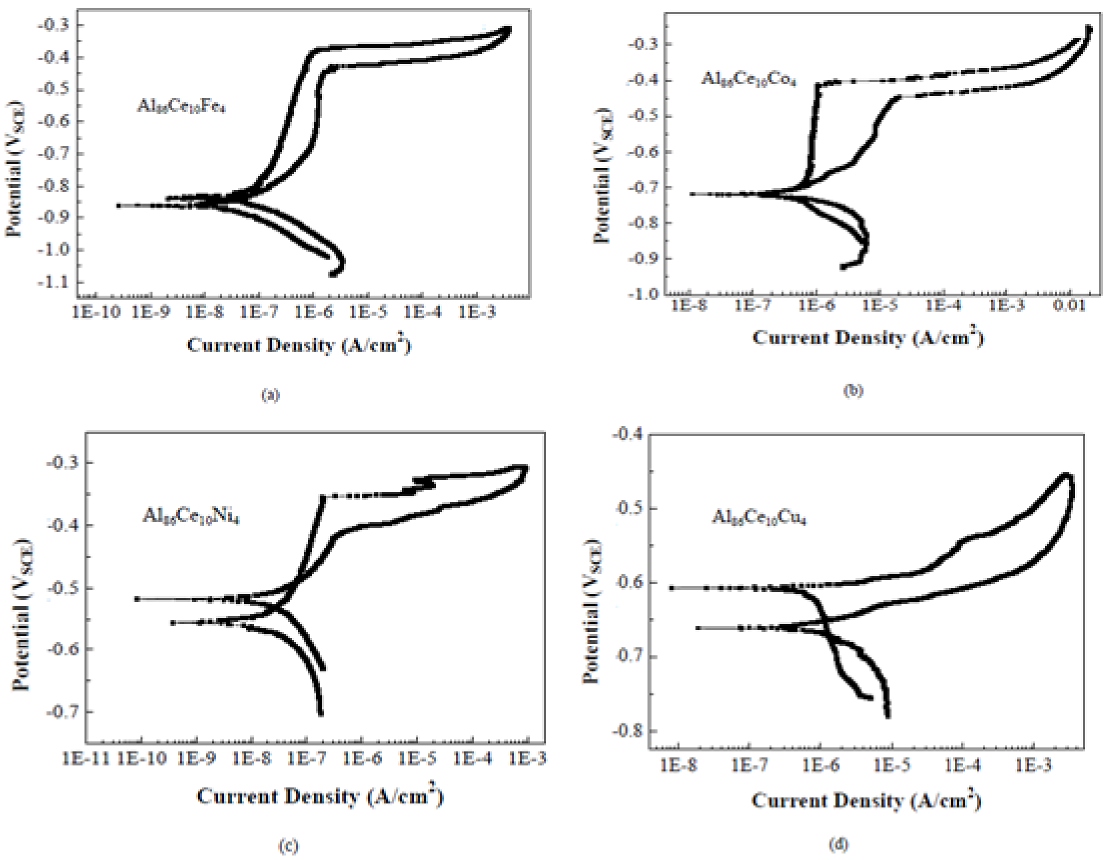

Figure 1: Electrochemical polarizations of the as-spun amorphous Al86Ce10TM4 (TM= Fe (a), Co (b), Ni (c), and Cu (d) alloys in 3.56 wt.% NaCl solution.

Annealing usually spurs nucleation and growth of metallic nano-crystals that are precipitated in the amorphous matrix, generating a composite texture consisting of both glassy phase and crystalline precipitates till the matrix develops into full polycrystalline phases. As seen from **Figure 2**, the electrochemical characterization evolves with the annealing crystallization process, and both corrosion resistance and mechanical hardness rise initially up to a maximum value (corresponding to an ideal texture with uniformly distributed nano-crystals tessellated in amorphous matrix) then falls monotonously to the value as the traditional Al polycrystalline alloys.

Table 1: Electrochemical data and hardness measured from the as-spun, post-annealed and post-oxidized Al86Ce10TM4 (TM= Fe, Co, Ni and Cu) alloys.

Alloys	T (oC)	Ecorr	Icorr	Ipass	Epit	Erep	∆ Erep	∆ Epass	Hv
		(VSCE)	(µA/cm2)	(µA/cm2)	(VSCE)	(VSCE)	(VSCE)	(VSCE)	(MPa)
Pure Al [17]	25	-1.10 ± 0.04	0.4 ± 0.2	1.5 ± 0.3	-0.74 ± 0.01	-1.14 ± 0.00	0.40 ± 0.01	0.36 ± 0.02	-
	25	-0.87 ± 0.01	0.08 ± 0.00	0.64 ± 0.05	-0.38 ± 0.01	-0.45 ± 0.01	0.07 ± 0.02	0.49 ± 0.02	863 ± 17
Al86Ce10Fe 4	304	-0.91 ± 0.02	0.03 ± 0.01	0.02 ± 0.01	-0.66 ± 0.02	-0.86 ± 0.02	0.20 ± 0.02	0.25 ± 0.02	1165 ± 20
Anneal	350	-0.85 ± 0.02	0.02 ± 0.01	0.03 ± 0.02	-0.75 ± 0.02	-0.88 ± 0.01	0.13 ± 0.03	0.10 ± 0.03	984 ± 16
	420	-0.93 ± 0.01	0.02 ± 0.01	0.08 ± 0.02	-0.77 ± 0.01	-0.86 ± 0.02	0.09 ± 0.03	0.16 ± 0.02	1033 ± 18
	10 h	-0.75 ± 0.06	8.0 ± 0.3	8.5 ± 0.3	-0.75 ± 0.02	-0.82 ± 0.05	0.07 ± 0.06	0.55 ± 0.02	848 ± 30
	20 h	-0.75 ± 0.05	4.0 ± 0.1	6.0 ± 0.3	-0.74 ± 0.03	-0.78 ± 0.04	0.04 ± 0.04	0.41 ± 0.05	707 ± 28
	50 h	-0.79 ± 0.04	4.6 ± 0.1	6.0 ± 0.3	-0.78 ± 0.02	-0.72 ± 0.02	0.06 ± 0.02	0.42 ± 0.02	650 ± 18
Al86Ce10Fe 4	100 h	-0.75 ± 0.10	0.7 ± 0.2	5.0 ± 0.3	-0.75 ± 0.05	-0.73 ± 0.06	0.02 ± 0.02	0.45 ± 0.04	559 ± 24
630oC	200 h	-0.73 ± 0.08	1.9 ± 0.4	7.0 ± 0.2	-0.73 ± 0.04	-0.78 ± 0.04	0.05 ± 0.03	0.42 ± 0.03	612 ± 18
oxidation	1000 h	-0.73 ± 0.06	2.0 ± 0.2	1.0 ± 0.3	-0.73 ± 0.02	-0.79 ± 0.03	0.06 ± 0.02	0.67 ± 0.02	646 ± 24
	2000 h	-0.75 ± 0.04	2.0 ± 0.2	2.0 ± 0.2	-0.75 ± 0.03	-0.78 ± 0.02	0.03 ± 0.03	0.65 ± 0.03	806 ± 18
	25	-0.71 ± 0.00	0.8 ± 0.2	1.0 ± 0.2	-0.44 ± 0.02	-0.45 ± 0.01	0.01 ± 0.03	0.27 ± 0.02	762 ± 20
Al86Ce10Co 4	284	-0.67 ± 0.03	0.3 ± 0.1	1.0 ± 0.2	-0.63 ± 0.02	-0.78 ± 0.02	0.15 ± 0.04	0.04 ± 0.02	1186 ± 18
Anneal	300	-0.68 ± 0.02	0.6 ± 0. 2	10 ± 2	-0.63 ± 0.02	-0.78 ± 0.02	0.15 ± 0.02	0.05 ± 0.02	1167 ± 16
	370	-0.66 ± 0.03	1.0 ± 0.2	10 ± 2	-0.63 ± 0.02	-0.80 ± 0.02	0.17 ± 0.04	0.03 ± 0.02	1053 ± 15
	25	-0.54 ± 0.02	0.10 ± 0.08	0.8 ± 0.3	-0.38 ± 0.02	-0.43 ± 0.02	0.05 ± 0.04	0.16 ± 0.02	809 ± 16
Al86Ce10Ni 4	250	-0.46 ± 0.02	0.08 ± 0.02	0.3 ± 0.1	-0.35 ± 0.02	-0.50 ± 0.02	0.15 ± 0.04	0.11 ± 0.02	1066 ± 22
Anneal	300	-0.55 ± 0.03	0.05 ± 0.02	0.3 ± 0.2	-0.38 ± 0.02	-0.50 ± 0.02	0.12 ± 0.04	0.17 ± 0.02	912 ± 16
	380	-0.71 ± 0.02	3.0 ± 0.6	-	-	-	-	-	840 ± 18
	10 h	-0.78 ± 0.04	8.0 ± 0.3	8.0 ± 0.3	-0.77 ± 0.05	-0.77 ± 0.03	0.00 ± 0.02	0.33 ± 0.02	1030 ± 18
Al86Ce10Ni 4	20 h	-0.79 ± 0.02	8.0 ± 0.3	9.0 ± 0.3	-0.76 ± 0.03	-0.69 ± 0.02	0.07 ± 0.02	0.34 ± 0.03	942 ± 22
630 oC	50 h	-0.78 ± 0.03	8.0 ± 0.3	8.0 ± 0.4	-0.77 ± 0.02	-0.78 ± 0.04	0.01 ± 0.01	0.33 ± 0.02	542 ± 20
oxidation	100 h	-0.76 ± 0.02	6.0 ± 0.3	7.0 ± 0.3	-0.78 ± 0.04	-0.78 ± 0.04	0.00 ± 0.02	0.32 ± 0.04	476 ± 16
	200 h	-0.77 ± 0.03	2.2 ± 0.3	5.5 ± 0.3	-0.78 ± 0.02	-0.78 ± 0.02	0.00 ± 0.02	0.32 ± 0.02	576 ± 22
	25	-0.62 ± 0.01	1.0 ± 0.2	20 ± 8	-0.54 ± 0.04	-0.65 ± 0.03	0.11 ± 0.07	0.08 ± 0.02	715 ± 11
Al86Ce10Cu 4	219	-0.65 ± 0.02	0.2 ± 0.1	10 ± 2	-0.55 ± 0.02	-0.75 ± 0.02	0.2 ± 0.04	0.10 ± 0.02	1020 ± 18
Anneal	270	-0.73 ± 0.02	4.0 ± 0.8	20 ± 4	-0.70 ± 0.02	-0.74 ± 0.02	0.04 ± 0.04	0.03 ± 0.02	880 ± 15
	350	-0.67 ± 0.03	4.0 ± 1.0	40 ± 10	-0.63 ± 0.03	-0.89 ± 0.02	0.26 ± 0.04	0.04 ± 0.02	720 ± 14

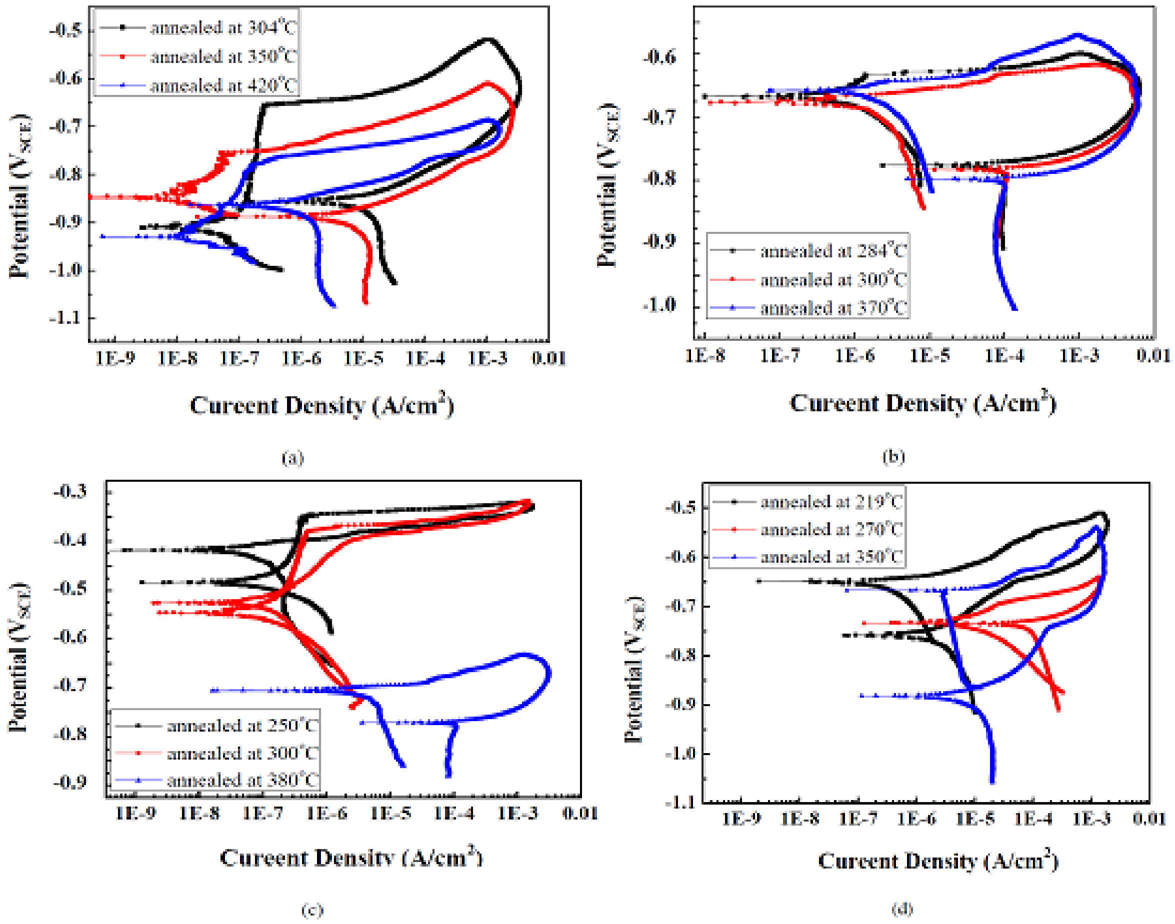

Figure 2: Electrochemical polarizations of the post-annealed Al86Ce10TM4 (TM=Fe (a), Co (b), Ni (c) and Cu (d)) alloys in 3.56 wt. % NaCl solution.

This encourages exploring what are the ideally optimized textures bearing the best mechanical and electrochemical properties and what mechanisms are laid on such textures with the unique properties. From **Figure 2 and Table 1**, even higher mechanical hardness and corrosion resistance can be achieved after amorphous matrix be annealed at peculiar temperatures for a certain of time, e.g. Al86Ce10Co4 annealed at temperature between 304~420°C, Al86Ce10Co4 at 284~370°C, Al86Ce10Ni4 at 250-300°C, and Al86Ce10Cu4 at 219°C for 15 min, respectively. The increment in mechanical hardness for the post-annealed alloys over their full amorphous texture relies on the fact that the precipitate hardening by sediment of metallic nano-crystals in the amorphous matrix is an added strengthening contributed to the amorphous matrix.

On the other hand, the improvement of electrochemical corrosion resistance for the post-annealed alloys over their amorphous matrix stands by the added anti-corrosion enhancement from the metallic nano-crystalline precipitates because majority of the precipitates are FCC-Al and Al11Ce3 nano-crystals, which are natively high self-passivating and corrosion resistant [18-22]. Further devitrification *via* annealing passing over the ideal textures incurs coarsening of the polycrystalline precipitates, thus both mechanical hardness and corrosion resistance diminish not only because the larger-sized crystals lesson the strengthening effects but arises distinct electrochemical inhomogeneities between the polycrystalline phases. As a consequence, understanding the devitrification process can greatly help to design, fabricate and engineer ideal structures for advanced materials.

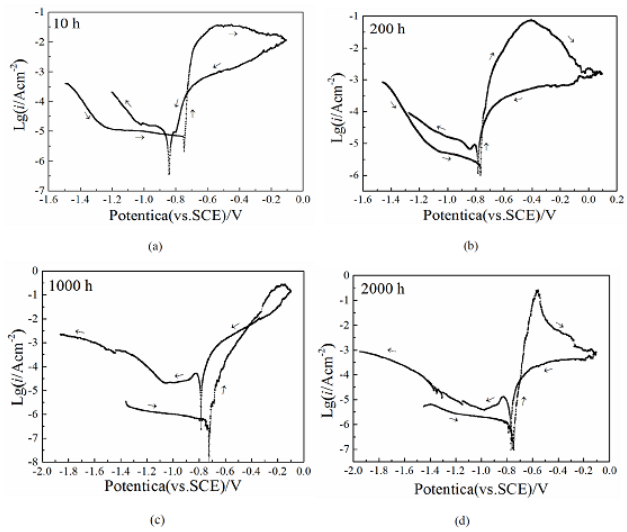

Figure 3: Polarization curves of the oxide films grown on as-spun Al86Ce10Fe4 at 630 °C in static air for (a) 10, (b) 200, (c) 1000, and (d) 2000 hours.

We have discussed the electrochemical behavior of the Al86Ce10TM4 (TM=Fe, Co, Ni and Cu) amorphous alloys and their crystallizations.

As discussed, annealing results in devitrification of the amorphous matrix; once crystallization rides over the ideal texture, mechanical and electrochemical properties fall and finally stay at the full polycrystalline state.

How the alloys behave under high temperature oxidation and how the oxide films perform under corrosion environment. The as-spun Al86Ce10TM4 (TM=Fe and Ni) amorphous alloys were oxidized at 630°C in static air for up to 2000 hours. Electrochemical polarizations of the oxide films grown on the alloys are present in **Figures 3 and 4**, respectively. The measured electrochemical data and mechanical hardness are tabulated in **Table 1**.

As seen from **Figures 3 and 4**, the oxides grown on the alloys at 630°C exhibit great blocking effect and resistance to corrosion in that corrosion current densities (Icorr and Ipass) rate low as 10-6 A/cm2, passivation regions (ΔEpass) span to 300-600 mV, and susceptibility to localized corrosion (ΔErep) are minor in 0-70 mV. The electrochemical behavior of the oxide films grown on the alloys shows much better corrosion resistance than the own alloys given the alloys are annealed at the same temperatures for the same period of time. The thickness of the oxide films grows with oxidation time and the thicken oxide films present higher corrosion resistance than the thinner, indicating the growing oxide films tend to be more compact, inert and resistant to corrosion.

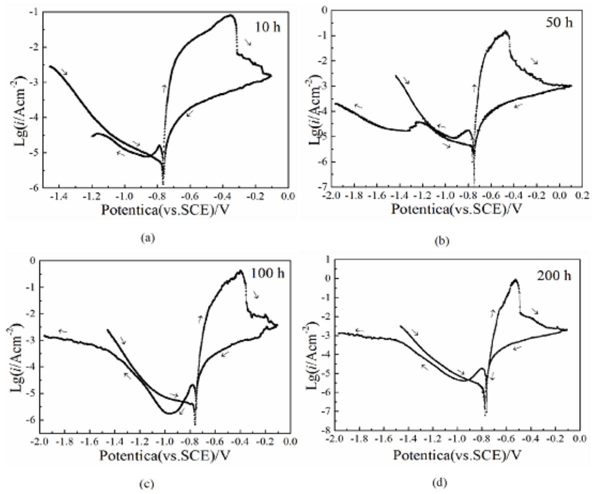

Figure 4: Polarization curves of the oxide films grown on as-spun Al86Ce10Ni4 at 630°C in static air for (a) 10, (b) 50, (c) 100, and (d) 200 hours.

Conclusion

Electrochemical behavior of the as-spun, post-annealed and post-oxidized Al86Ce10TM4 (TM=Fe, Co, Ni and Cu) alloys was investigated. The corrosion resistance and mechanical hardness of the amorphous alloys are substantially higher than the traditional Al alloys on merit of the uniqueness of the amorphous textures. Devitrification enables to raise the properties significantly to the maximum values by ideally precipitating uniformly-distributed nanocrystals in the amorphous matrix. The oxide films grown on the alloys present good corrosion resistance. The results manifest the amorphous Al86Ce10TM4 (TM=Fe, Co, Ni and Cu) alloys exhibit corrosion resistance and mechanical hardness much superior to the traditional Al alloys in terms of mechanical strength (800~1200 MPa), high temperature endurance (300~420°C), oxidation (630°C) and corrosion resistance (10-6~10-8 A/cm2) of the former comparing to the strength (550 MPa), temperature endurance (200°C), and corrosion resistance (10-6A/cm2) of the latter, therefore mark potential values for aerospace and national defence.

Acknowledgements

This work was supported by National Natural Science Foundation of China under the grants of NNSF Nos. 50642034, 20963006, 51061012, 51161014 and 51761035; the Ministry of Science and Technology of China under the grant No. of 2012DFA51260; and the Inner Mongolia Key Natural Science Foundation of China under the grant No. of 2017ZD03. The authors gratefully acknowledge the above financial supports.

References

1. He Y, Poon SJ, Shiflet J (1988) Synthesis and properties of metallic glasses. J Aluminum Science 241: 1640–1642.

2. Inoue A, Ohtera K, Tsai AP, Masumoto T, Pn J (1988) New amorphous Mg-Ce-Ni alloys with high strength and good ductility. J Appl Phys: 27:12.

3. Johnson WL (1988) Crystal-to-glass transformation in metallic materials. Mater Sci Eng 97: 1–13.

4. Inoue A (1998) Amorphous, nanoquasicrystalline and nanocrystalline alloys in Al-based systems. Progress in Material Science 43: 365-520.

5. Wang WH, Dong C, Shek CH (2004) Bulk metallic glasses. Mater Sci Eng R 44: 45-98.

6. Polk DE(1972) The structure of glassy metallic alloysStructure des alliages metalliques vitreuxDie struktur glasähnlicher metallischer Legierungen. Acta Metall 20: 485–491.

7. Whang SH (1983) New prediction of glass-forming ability in binary alloys using a temperature-composition map. Mater Sci Eng 57: 87–95.

8. Malekan M, Shabestari SG, Gholamipour R, Seyedein SH (2009) Effect of Ge addition on mechanical properties and fracture behavior of Cu–Zr–Al bulk metallic glass. J Alloys Compd 484: 708–711.

9. Salehi M, Shabestari SG, Boutorabi SMA (2013) Glass-forming ability, thermal stability, mechanical and electrochemical behavior of Al-Ce-TM (TM = Ti, Cr, Mn, Fe, Co, Ni and Cu) amorphous alloys. Mater Sci Eng A 586: 407–412.

10. Shen Y, Perepezko JH (2017) Al-based amorphous alloys: Glass-forming ability, crystallization behavior and effects of minor alloying additions. J Alloys Compd 707: 3-11.

11. Rusanov B, Sidorov V, Svec P, Janckovic D, A Moroz A et al. (2019) Electric properties and crystallization behavior of Al-TM-REM amorphous alloys. J Alloys Compd 787: 448-451.

12. El-Jaby S, Lewis BJ, Tomi L(2019) A commentary on the impact of modelling results to inform mission planning and shield design Life Sciences in Space Research.

13. Sweitzer JE, Shiflet GJ, Scully JR (2003) Localized corrosion of Al90Fe5Gd5 and Al87Ni8.7Y4.3 alloys in the amorphous, nanocrystalline and crystalline states: resistance to micrometer-scale pit formation. Electrochim Acta 48: 1223–1234.

14. Lucente AM, Scully (2007) Pitting and alkaline dissolution of an amorphous−nanocrystalline alloy with solute-lean nanocrystals. Corros Sci 49: 2351–2361.

15. GH Li, Wang WM, HJ Ma, Li RZH, et al. (2011) Effect of different annealing atmospheres on crystallization and corrosion resistance of Al86Ni9La5 amorphous alloy. Mater Chem Phys 125:136–142.

16. Wang JQ, Liu YH, Imhoff S, Chen N, DV Louzguine-Luzgin et al. (2012) Enhance the thermal stability and glass forming ability of Al-based metallic glass by Ca minor-alloying. A Inoue Intermetallics 29: 35–40.

17. Zhang J, Shi P, Chang A, Zhao T, Li W, et al. (2019) Glass-forming ability, thermal stability, mechanical and electrochemical behavior of Al-Ce-TM (TM = Ti, Cr, Mn, Fe, Co, Ni and Cu) amorphous alloys. J Non-Cryst Solids X1 100005.

18. Zhang J, Chang C,A Chang A, Zhao T, Jia J e al. (2019) Int. J Nanotechnol Nanomed 4: 1–12.

19. Birbilis N, Buchheit RG (2005) Electrochemical characteristics of intermetallic phases in aluminum alloysan experimental survey and discussion. J Electrochem Soc 152: B140-B151.

20. Zhu L, Soto-Medina S, Hennig RG, Manuel MV (2019) Experimental investigation of the Al−Co−Fe phase diagram over the whole composition range. J Alloys and Compd.

21. Zhu L, Soto-Medina S, Cuadrado-Castillo W, Hennig RG, Manuel MV (2019) New experimental studies on the phase diagram of the Al-Cu-Fe quasicrystal-forming system. J Alloys and Compd.

22. Su J, Guo F, Cai H, Liu L(2019) Structural analysis of Al−Ce compound phase in AZ-Ce cast magnesium alloy. Journal of Materials Research Technology 8: 6301-6307.